Int J Adv Manuf Technol (2007) 31: 705–715
DOI 10.1007/s00170-005-0240-5

ORIGINAL ARTICLE

Lee-Ing Tong · Chung-Ho Wang · Da-Lun Chen

Development of a new cluster index for wafer defects

Received: 24 May 2005 / Accepted: 26 August 2005 / Published online: 13 April 2006

Abstract Defect number and defect clustering are two key determinants of wafer yield. Preventing and detecting wafer defects thus is an important issue in integrated circuit manufacturing. Defect clustering tends to grow with increasing wafer size. Methods have been developed for assessing defect clustering on wafers. However, these methods require either statistical assumptions regarding defect distribution or complex computations. This study develops a new cluster index, utilizing the rotating axis technique from multivariate analysis to accurately quantify defect clusters on a wafer. The developed defect-clustering index does not require making assumptions regarding defect distribution. Thus, the proposed method can be efficiently used by engineers with little statistical background. A simulation experiment is conducted to demonstrate the effectiveness of the proposed defect-clustering index.

Keywords Integrated circuit · Wafer · Defect clustering · Rotation of axes · Multivariate analysis

1 Introduction

Fierce global competition has led integrated circuit (IC) manufacturers to strive to increase product yield. Because wafer yield significantly influences productivity, improving wafer yield is important for IC manufacturers. The number of defects per wafer is the primary determinant of wafer yield. Wafer yield decreases with increasing number of defects. However, if wafer defects display clustering, the number of defects per wafer may not reflect actual yield. Consequently, besides the number of defects, the degree of defect clustering on a wafer also must be assessed to accurately reflect defect distribution and thus enhance wafer yield.

Defect clustering increases with increasing wafer size. Consequently, the conventional Poisson yield model based on the Poisson distribution tends to underestimate yield. Stapper [6] thus proposed a negative binomial yield model that can estimate wafer yield more accurately than the conventional yield model. The negative binomial yield model is used extensively in the IC industry because it simultaneously accounts for the number of defects and defect clustering (using clustering index α). However, the range of α values is scattered and sometimes is negative [1] making it difficult for engineers to assess degree of defect clustering. Jun et al. [3] designed a clustering index (denoted by CI_J) for assessing the degree of defect clustering on a wafer and confirmed that the CI_J can represent defect clustering more accurately than the α obtained from a binomial negative distribution. Although the CI_J does not require any statistical assumptions regarding the defect distribution, CI_J may yield consistent values for various types of defect distributions formed on wafers. These consistent values confirm that the CI_J may address erroneous judgments when assessing the degree of defect clustering.

This study designed a new clustering index, CI_M, using the rotating axis technique from multivariate analysis [7], to overcome the drawbacks of the CI_J. The CI_M possesses the same advantage as the CI_J in not requiring assumptions regarding the defect distribution. Moreover, the CI_M can also represent defect clustering on a wafer more accurately than the CI_J. Simulation experiments were conducted to compare the proposed CI_M and other existing cluster indices for application in IC fabrication. These simulations verified the effectiveness of the proposed method.

L.-I. Tong
Department of Industrial Engineering and Management,
National Chiao Tung University,
HsinChu, Taiwan, Republic of China

C.-H. Wang (✉)
Department of Computer Science,
Chung Cheng Institute of Technology,
National Defense University,
Taoyuan, Taiwan, Republic of China
e-mail: wch@ccit.edu.tw

D.-L. Chen
Total Quality Management Committee,
United Microelectronic Corporation,
HsinChu, Taiwan, Republic of China

Table 1 α values from the negative binomial model and the corresponding imitated yield models [1]

Clustering	α value	Yield model
None	10 or greater	Poisson
Some	4.2	Murphy
Some	3	Dingwall
Much	1	Seeds

2 Literature review

2.1 Defect clustering indices

The conventional yield model assumes that the number of defects on a wafer follows a Poisson distribution. This assumption implies that the defects display a random distribution. However, defects tend to be clustered rather than dispersed randomly over a wafer. Consequently, certain spatial distributions related to wafer defects, including a compound Poisson distribution and generalized Poisson distribution, were considered in establishing a yield model. The negative binomial model, as follows, is probably the best known.

$$Y = \frac{1}{(1 + D_0 A/\alpha)^{\alpha}} \tag{1}$$

where Y denotes the yield, D_0 represents the average number of defects per unit area, A is the chip area, and α is the clustering parameter $\alpha = \overline{\lambda}^2 \Big/ \left(\sigma^2 - \overline{\lambda}\right)$, where $\overline{\lambda}$ and σ^2 denote the mean and variance of defects per die, respectively. A smaller α value corresponds to a larger variation in the defect density on a wafer.

Cunningham [1] noted that the α values obtained directly from the equation $\alpha = \overline{\lambda}^2 \Big/ \left(\sigma^2 - \overline{\lambda}\right)$ can be quite scattered and sometimes negative. Cunningham [1] also showed that the compound yield equations could be closely imitated by selecting α values. Table 1 lists the α values and corresponding imitated yield models. For more developed compound yield models, see Raghavachari [5].

Rogers [4] developed the quadrat method for analyzing the point spatial distribution. The quadrat method involves initially dividing the plane surface into numerous equal-sized grids. The random defect distribution in each grid then is assessed. If the defects are randomly distributed on the plane surface, the defects on each grid then are also randomly distributed and follow a Poisson distribution. The variance-mean ratio (V/M) value associated with each grid is one when the defects follow a Poisson distribution. The V/M value exceeds one if the defects are clustered. The V/M values can be proven to possess a t distribution with $n-1$ degrees of freedom. The defects are clustered on each grid once the V/M value exceeds the critical t_{n-1} point. t_{n-1} can be expressed as follows.

$$t_{n-1} = (V/M - 1)\sqrt{\frac{2}{n-1}} \tag{2}$$

where n denotes number, while V and M represent the variance and mean of defects per wafer, respectively. Besides the V/M index, other clustering indices based on the quadrat method also have been developed. The performance of these clustering indices varies markedly with grid size, grid determination method and grid shape given a particular defect distribution.

Jun et al. [3] designed a clustering index (CI_J) to assess the degree of defect clustering on a wafer. The simulation results showed that the CI_J represents defect clustering more accurately than the α from the well-known negative binomial distribution. The CI_J value is independent of the chip area, requires no assumptions regarding the defect distribution, and is easy to calculate. Suppose that n defects exist on a wafer, employing the x and y coordinates, the ith defect can be denoted using (x_i, y_i), where i=1, 2, ..., n. Accordingly, all of the defects can be projected onto the x and y coordinates. Figure 1 illustrates examples of defect maps and the corresponding projected x and y coordinates.

The defect intervals on the x and y coordinates are defined as follows [3].

$$V_i = x_i - x_{i-1}, \quad i = 1, 2, ..., n \tag{3}$$

$$W_i = y_i - y_{i-1}, \quad i = 1, 2, ..., n \tag{4}$$

where x_0=y_0=0 and x_i and y_i represent the ith and the yth smallest values, respectively. From Fig. 1d, defect clustering tends to display burstiness or clumps in the x and y coordinates. This type of defect cluster creates a large

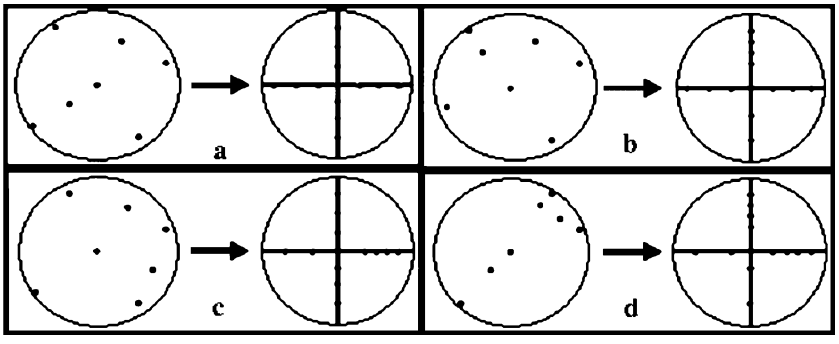

Fig. 1 **a**–**d** Defect maps and projected x and y coordinates [3]

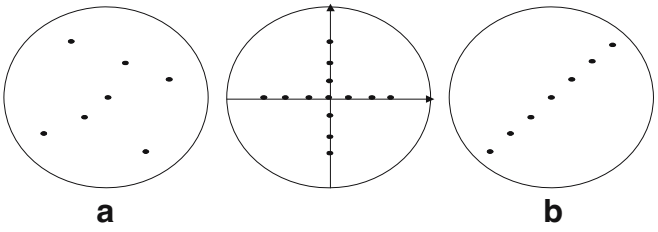

Fig. 2 **a**, **b** Defect maps and projected x and y coordinates

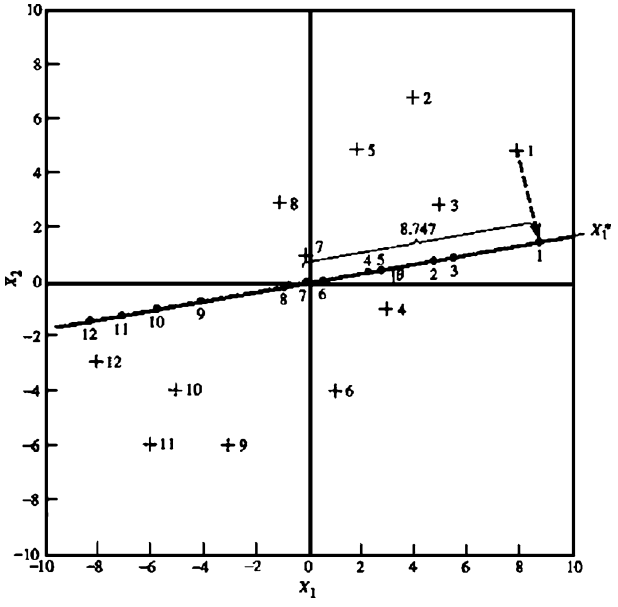

Fig. 3 Expression of rotating axis [7]

variance regarding the defect intervals. However, Fig. 1b and c show that burstiness on either the x- or y-axis does not necessarily represent clustered defects. Based on the relationship between the defect clustering and cluster burstiness or clumps in the x and y coordinates, Jun et al. [3] designed the CI_J, as follows.

$$CI_J = \min\left\{\frac{S_v^2}{\overline{V}^2}, \frac{S_w^2}{\overline{W}^2}\right\} \tag{5}$$

where $\overline{V} = \sum V_i/n$; $S_v^2 = \sum \left(V_i - \overline{V}\right)^2 \Big/ (n-1)$; $\overline{W} = \sum W_i/n$ and $S_w^2 = \sum \left(W_i - \overline{W}\right)^2 \Big/ (n-1)$. If the defect locations are assumed to be uniform random variables, the CI_J approaches 1. A large CI_J value corresponds to highly clustered defects. Despite the advantage that the CI_J requires no statistical assumptions regarding defect distribution, it still suffers some drawbacks, as shown in Fig. 2. Figure 2a,b display consistent CI_J values based on Eq. 5, but display different types of defect distributions. Specifically, one distribution is randomly distributed and the other has a patterned distribution. Accordingly, the CI_J cannot accurately assess the degree of defect clustering. This inability occurs because the CI_J values are calculated based on the projected defect coordinates associated with the x- and y-axes. Consequently, defect locations on a wafer cannot be depicted accurately. In this case, the CI_J could underestimate the degree of defect clustering.

2.2 Rotating axis technique [7]

Figure 3 presents an example of the application of the rotating axis technique. From Fig. 3, some points are located in a two-dimensional space (that is, x_1 and x_2) and a new coordinate x_1* is obtained by rotating the x_1 axis counterclockwise using θ^0, where $0 \le \theta \le 180$. Accordingly, these points in two-dimensional space can be projected into the new axis x_1*. The corresponding coordinates are determined as follows.

$$x_1{}^* = \cos\theta \times x_1 + \sin\theta \times x_2 \tag{6}$$

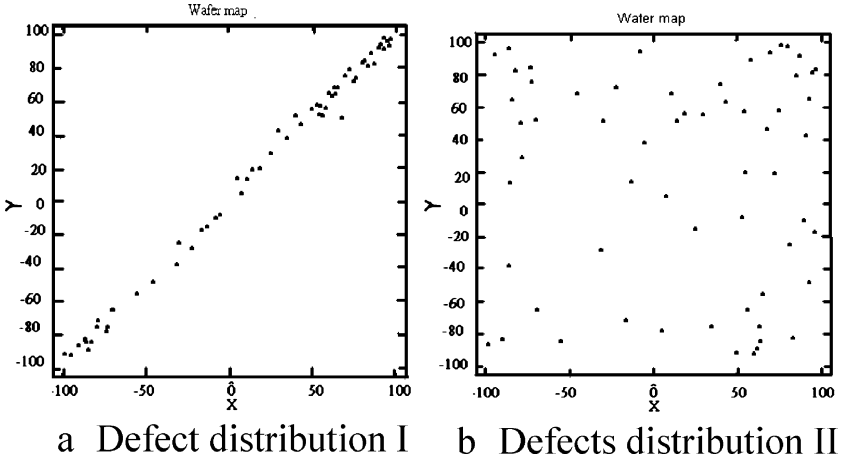

Fig. 4 Wafer map illustration. **a** Defect distribution I. **b** Defect distribution II

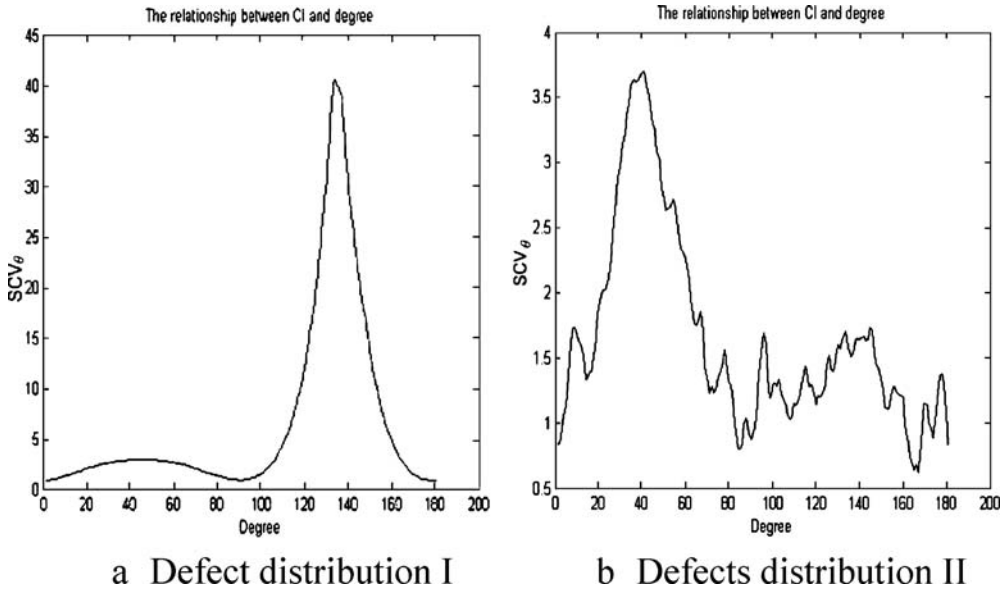

Fig. 5 Diagram of SCV_θ versus θ. **a** Defect distribution I. **b** Defect distribution II

3 Developed clustering index procedure

The developed CI_M includes the following five steps.

Step 1.

Project the defect coordinates (x_i, y_i) into a new axis obtained by rotating the x-axis counterclockwise using θ^0.

Suppose that a wafer has n defects, and (x_i, y_i) denotes the x and y coordinates of the ith defect location in a two-dimensional space, i=1, ...,n. These n defects then can be projected onto a new axis $x^*_{i,\theta}$ obtained by rotating the x-axis counterclockwise using θ^0. The new coordinates for the ith defect with respect to θ then can be calculated as follows [7].

$$x^*_{i,\theta} = \cos\theta \times x_i + \sin\theta \times y_i \tag{7}$$

where i denotes the ith defect and θ represents a rotating angle, where $0 \le \theta \le 180$.

Step 2.

Sort the $x^*_{i,\theta}$ values in ascending order and calculate the intervals between each adjacent coordinate value $x^*_{i,\theta}$.

The intervals between each adjacent coordinate value $x^*_{i,\theta}$ then can be calculated as follows.

$$v_{i,\theta} = x^*_{(i,\theta)} - x^*_{(i-1,\theta)} \tag{8}$$

where $x^*_{(0,\theta)} = 0$ and $v_{i,\theta}$ represents the ith interval between $x^*_{(i,\theta)}$ and $x^*_{(i-1,\theta)}$.

Step 3.

Calculate the squared coefficient of variation (SCV) for $v_{i,\theta}$.

The SCV for $v_{i,\theta}$ can be determined as follows.

$$SCV_\theta = \frac{s^2_{v,\theta}}{\overline{v}^2_\theta} \tag{9}$$

where SCV_θ represents the squared coefficient of variation for $v_{i,\theta}$; $\overline{v}_\theta = \left(\sum_{i=1}^{n} v_{i,\theta}\right) \Big/ n$, and $s^2_{v,\theta} = \left(\sum_{i=1}^{n} (v_{i,\theta} - \overline{v}_\theta)^2\right) \Big/ (n-1)$.

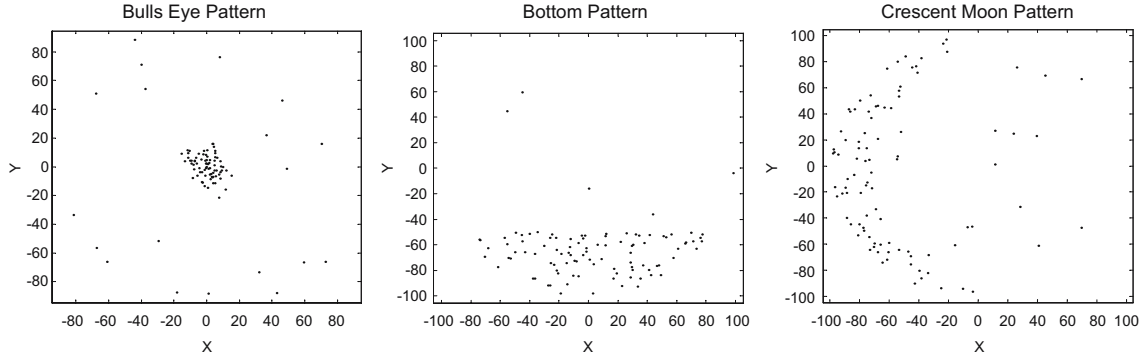

Fig. 6 Defect clustering maps for the bull's eye, bottom, and crescent moon patterns

Table 2 Factors/levels of the designed experiment

Pattern	Number of defects	Chip size	Defect percentage
Random	20, 50, 100, 150, 200, 300	5, 10, 20	–
Bull's eye pattern	20, 50, 100, 150, 200, 300	5, 10, 20	75%, 90%, 95%
Bottom pattern			
Crescent moon pattern			

Step 4.

Change the angle of θ and calculate the corresponding θ=1^0 value.

The number of 180 SCV_θ values with respect to θ, increased by θ=1^0, can be obtained through Steps 1–3.

Step 5.

Calculate the developed CI_M.

According to the SCV_θ values obtained from Step 4, the average SCV_θ value determines the clustering index CI_M, as follows.

$$CI_M = \frac{\sum_{\theta=0}^{180} SCV_\theta}{180} \tag{10}$$

where CI_M represents the developed clustering index. A larger CI_M value indicates a stronger degree of defect clustering formed on a wafer.

4 Comparison of the CI_M and CI_J

The CI_M and CI_J were compared using Fig. 4 to demonstrate the superiority of CI_M compared to CI_J. Figure 4a,b display clustered defects and a random defect distribution on respective wafer maps. The method developed by Jun et al. [3] produces a consistent CI_J value of 0.8354 while quantifying the degree of defects regarding these two wafer maps. From the CI_J properties, the uniform defect distribution yields a CI_J value of nearly 1. These two wafers exhibit consistent defect distributions. However, the defect distribution differs significantly between the two wafers. Consequently, the CI_J cannot accurately quantify defect clustering on a wafer.

The CI_M was also used to assess the degree of defect clustering in Fig. 4a,b. From the procedure developed for establishing the CI_M, the 180 SCV_θ values can be obtained via Steps 1–4. Figure 5a,b display the diagrams of corresponding SCV_θ values versus various θ values. Clearly, the SCV_θ values vary with θ. The maximum SCV_θ values in Fig. 5a,b are 41 and 3.7, and the corresponding CI_M are 6.6925 and 1.6632, respectively. Accordingly, this study concludes that the degree of defect clustering in Fig. 4a exceeds that in Fig. 4b. The developed CI_M therefore can more accurately assess defect clustering on a wafer than CI_J. Notably, CI_J is determined using CI_M, with θ=0^0 and θ=90^0, using the minimum squared coefficient of variation. The proposed procedure not only explains the SCV_0 and SCV_{90}, but also considers $0 \leq \theta \leq 180$ to obtain the CI_M for assessing defect clustering on a wafer. Therefore, the CI_M represents defect clustering more accurately than other indices.

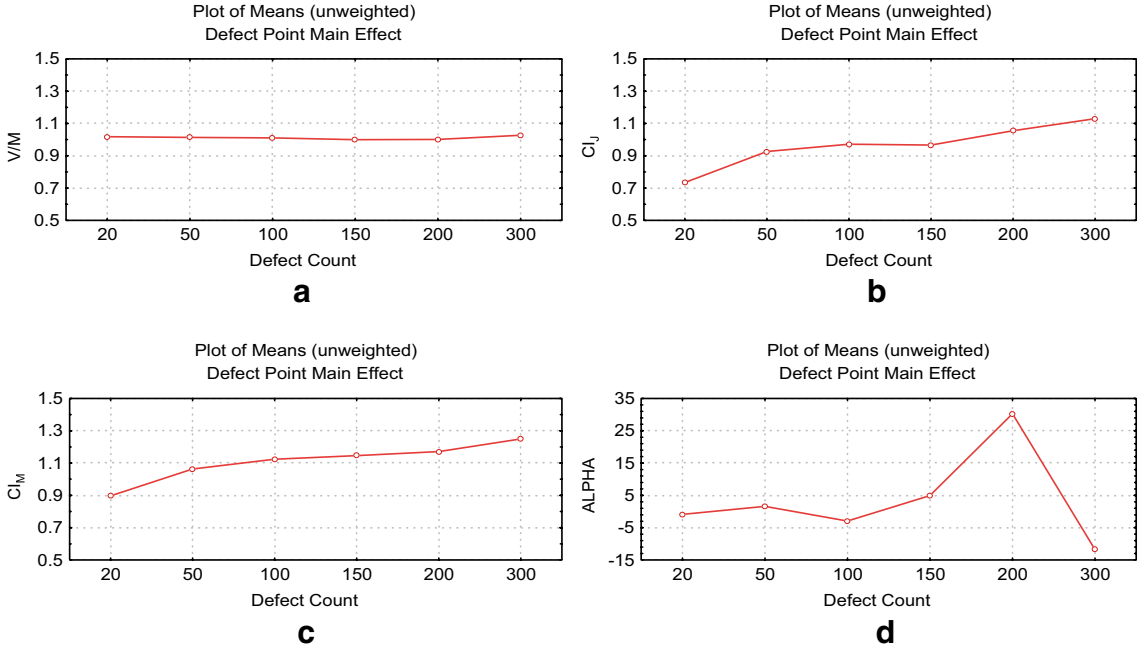

Fig. 7 **a**–**d** Effect of defect count for a random defect distribution on four clustering indices

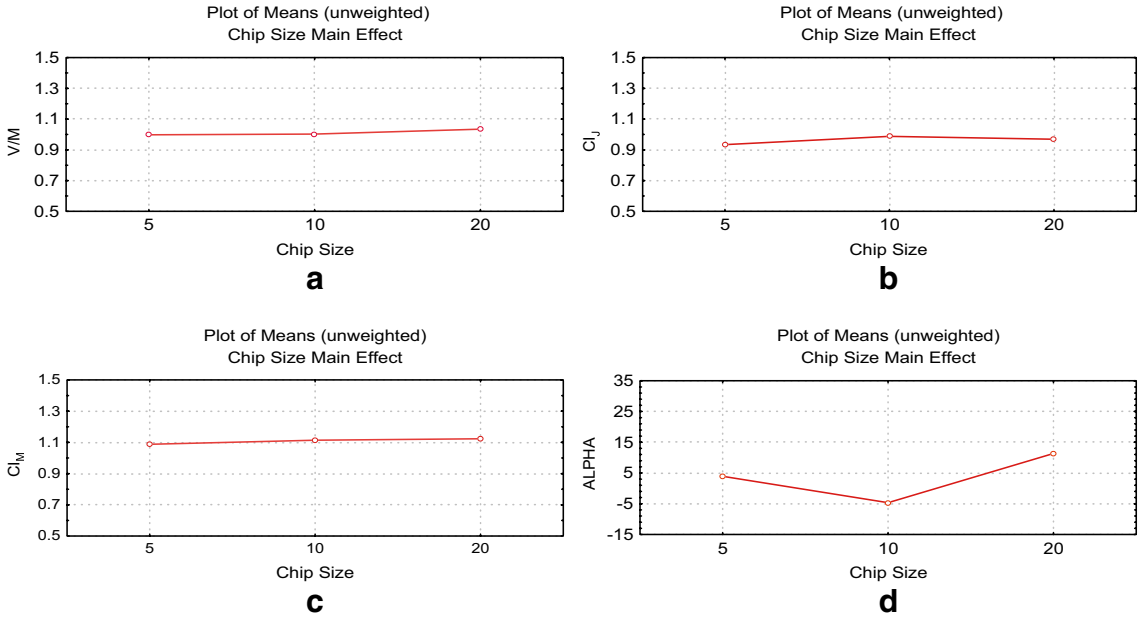

Fig. 8 **a**–**d** Effect of chip size for a random defect distribution on four clustering indices

5 Simulation experiments

An efficient defect-clustering index must be robust against various chip size and defect distributions and correctly assess defect clustering degree. Accordingly, an experiment design involving three common defect clustering patterns, including the bull's eye pattern, bottom pattern, crescent moon pattern [2] and no pattern (namely a random defect distribution following a Poisson distribution) were simulated on eight inch wafers to demonstrate the effectiveness of the developed CI_M. Figure 6 displays these three common defect clustering patterns. The experiment design included three factors, six levels for the number of defects, three levels for the chip size and three levels for the defect percentage contained in the clustering area. Table 2 lists these factors and levels, where 234 factor level combinations (runs) were generated using this approach; ten replicate runs were conducted, and 2,340 runs with different types of wafer maps thus were simulated. Accordingly, the α, CI_J, and CI_M values for each run were determined using Eqs. 1, 5 and 10, respectively.

Figures 7 and 8 display the defect count and chip size effects associated with a random defect distribution. From Figs. 7a–c and 8a–c, the V/M, CI_J and CI_M indices displayed the exceptional properties of being insensitive to defect count and chip size. The values of all of these indices

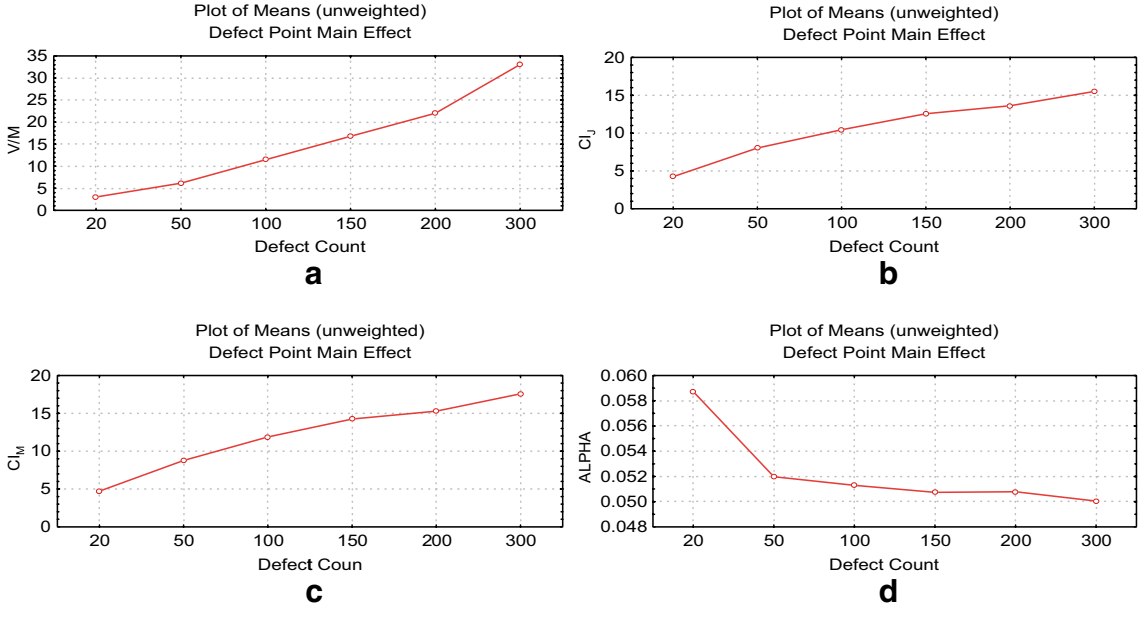

Fig. 9 **a**–**d** Effect of defect count for the bull's eye pattern on four clustering indices

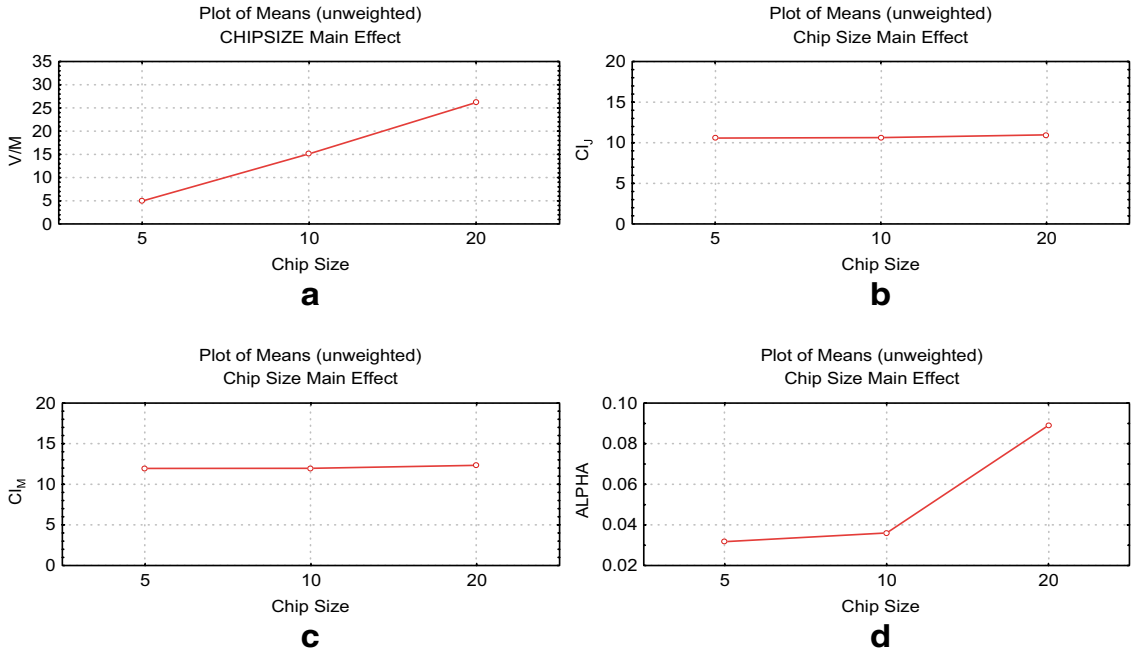

Fig. 10 **a**–**d** Effect of chip size for the bull's eye pattern on four clustering indices

approached one. However, from Figs. 7d and 8d, the α value had a strongly scattered pattern that varied with the defect count and chip size and sometimes was negative. The α value is inadequate for assessing the degree of defect clustering and is not robust to the defect count and chip size when the defects are randomly distributed.

Figures 9, 10 and 11 display the defect count, chip size and defect percentage effects associated with the bull's eye pattern, respectively. From Figs. 9a and 11a, the *V*/*M* index value increased with clustering degree. However, From Fig. 10a, the *V*/*M* index value altered with the chip size and did not display exceptional properties for a robust defect-clustering index. Figures 9d and 11d display that the α index values are located within a narrow range, creating difficulty in assessing the degree of defect clustering. From Fig. 10d, the α index varied with chip size and did not display exceptional properties. Figures 9c,d and 11c,d display that the CI_J and CI_R can efficiently assess the degree of defect clustering. Moreover, Fig. 10c and d reveal that both indices are robust to the chip size.

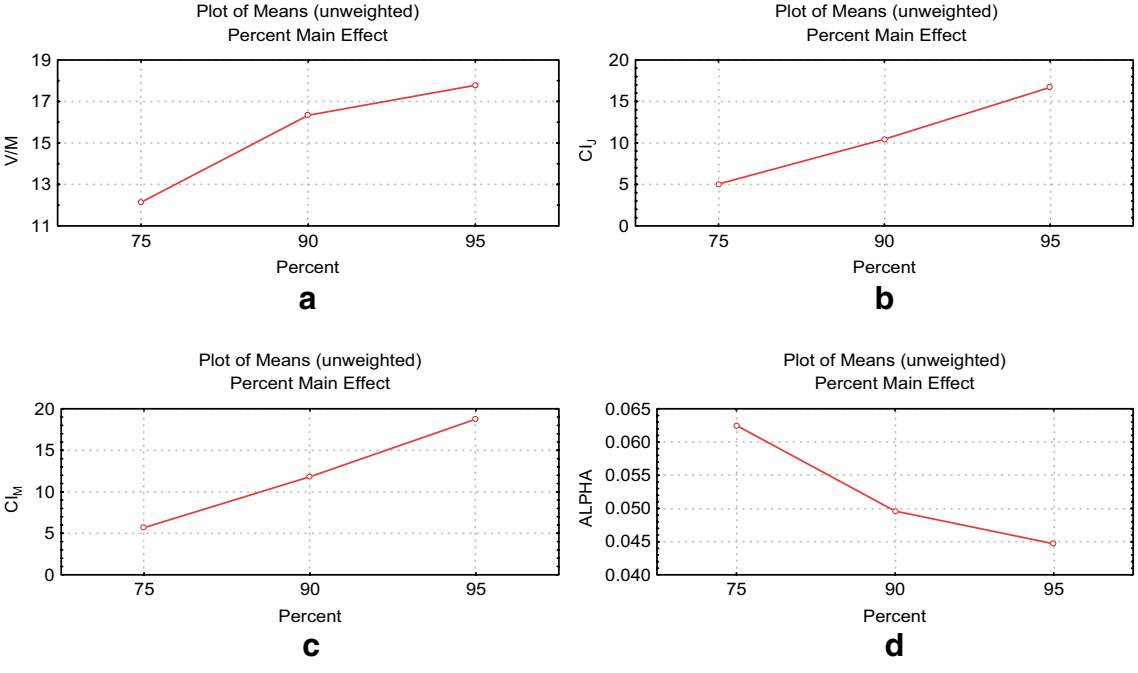

Fig. 11 **a**–**d** Effect of defect percentage for the bull's eye pattern on four clustering indices

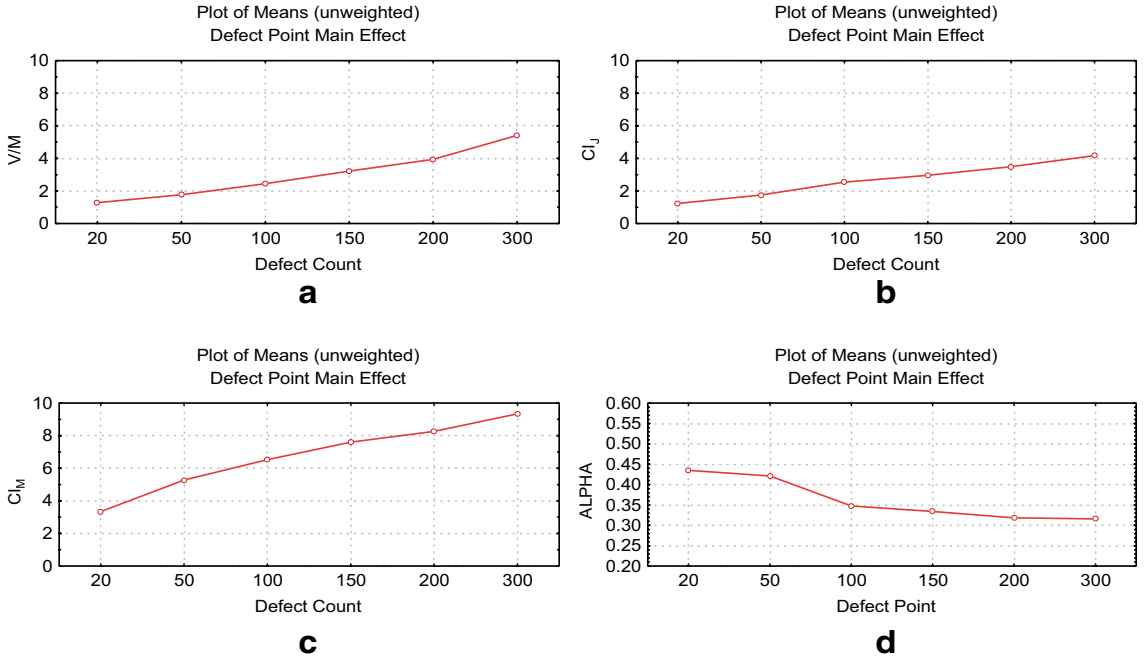

Fig. 12 **a**–**d** Effect of defect count for the bottom pattern on four clustering indices

Figures 12, 13 and 14 display the defect count, chip size and defect percentage effects associated with the bottom pattern, respectively. From Figs. 12c and 14c, the CI_M values increased with the defect count and percentage in the clustering area. The CI_M was insensitive to the chip size. The CI_M can accurately assess the degree of defect clustering. From Figs. 12b and 14b, although the CI_J values are insensitive to chip size, this index is insensitive to the percentage of defects in the clustering area. This index thus does not satisfy the required properties. From Fig. 13a,d, the V/M and α indices values vary with chip size. Consequently, CI_M is superior to CI_J, V/M and α for assessing defect clustering associated with the bottom pattern.

Figures 15, 16 and 17 illustrate the defect count, chip size and defect percentage effects associated with the crescent moon pattern, respectively. From Figs. 15c and 17c, the CI_M values are insensitive to the chip size. The CI_M

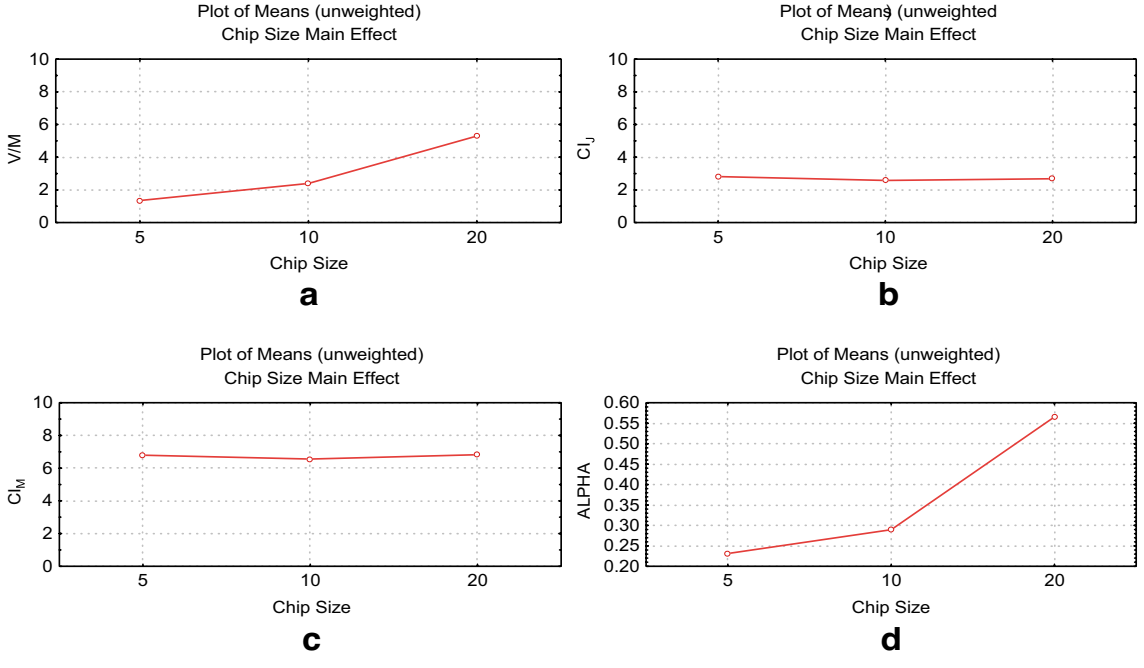

Fig. 13 **a**–**d** Effect of chip size for the bottom pattern on four clustering indices

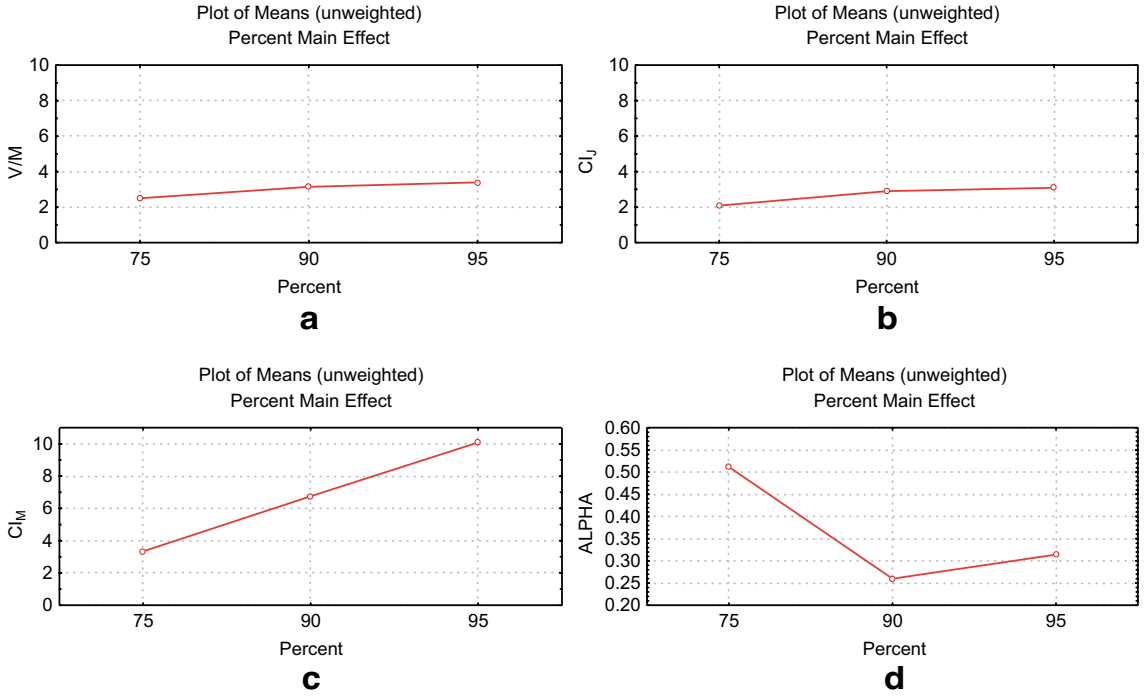

Fig. 14 **a**–**d** Effect of defect percentage for the bottom pattern on four clustering indices

values increase with the defect count and percentage of defects contained in the clustering area. Consequently, CI_M can accurately assess the degree of defect clustering in the crescent moon pattern. Figures 15b and 17b indicate that the CI_J values approach one. Accordingly, this study concludes that the defects are randomly distributed based on the discrimination of CI_J. However, actual defects on a wafer are not randomly distributed (instead displaying a crescent moon pattern). Therefore, CI_J cannot discriminate the degree of defect clustering and makes inaccurate judgments regarding the crescent moon pattern. From Fig. 16a,d, the values of the V/M and α indices vary with the chip size. Therefore, the CI_M is superior to the CI_J, V/M

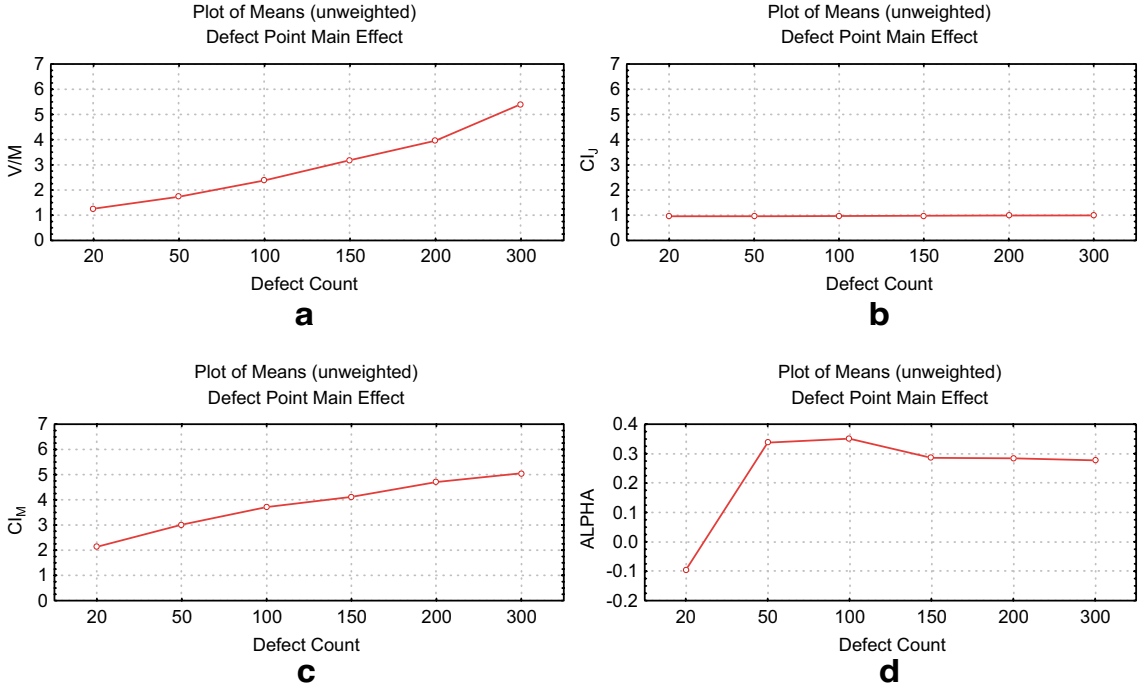

Fig. 15 **a**–**d** Effect of defect count for the crescent moon pattern on four clustering indices

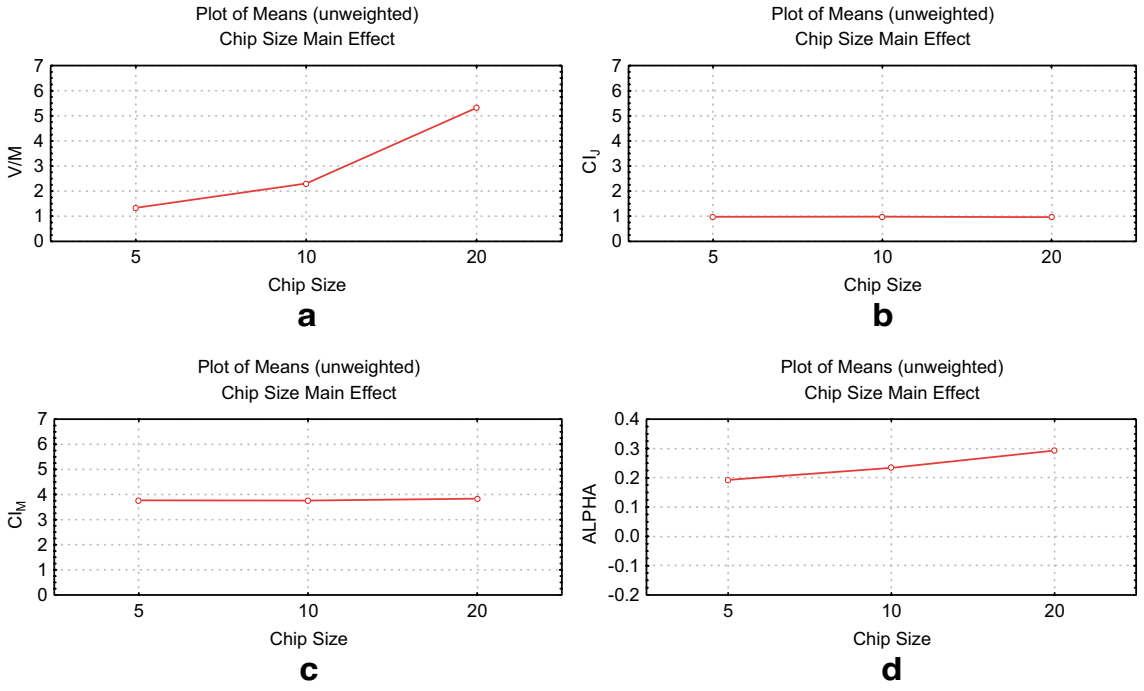

Fig. 16 **a**–**d** Effect of chip size for the crescent moon pattern on four clustering indices

and α indices for assessing defect clustering associated with the crescent moon pattern.

Table 3 summarizes comparisons of these four defect clustering indices, namely CI_M, CI_J, α and V/M, for assessing the random pattern, bull's eye pattern, bottom pattern and crescent moon pattern under three designed factors. To summarize, CI_M is superior to the other three indices. Consequently, the effectiveness of the developed clustering index for assessing the degree of defect clustering on a wafer is confirmed.

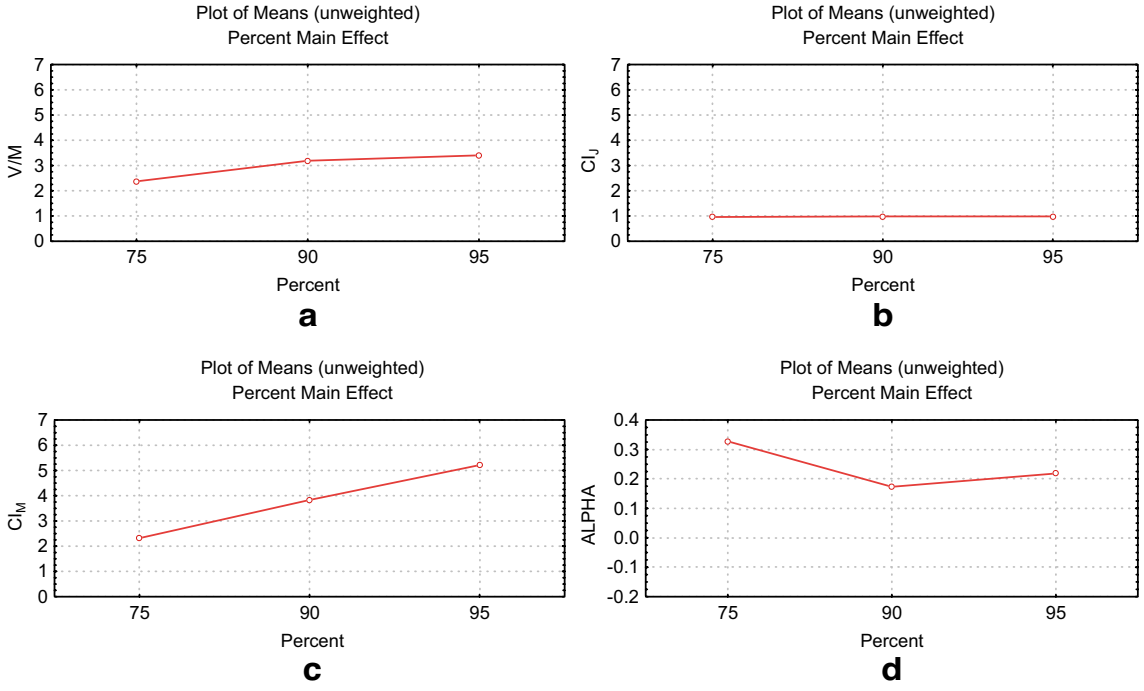

Fig. 17 **a**–**d** Effect of defect percentage for the crescent moon pattern on four clustering indices

Table 3 Comparisons of four defect clustering indices

	Number of defects				Chip size				Defects percentage			
	CI_M	CI_J	α	V/M	CI_M	CI_J	α	V/M	CI_M	CI_J	α	V/M
Random pattern	○	○	×	□	○	○	×	□	–	–	–	–
Bull's eye pattern	○	○	×	○	○	□	×	×	○	○	×	○
Bottom pattern	○	△	×	△	○	○	×	×	○	×	×	△
Crescent moon pattern	○	×	×	○	○	○	×	×	○	×	×	△

The ○ symbol represents the index with exceptional properties for assessing defect clustering

The △ symbol represents the index with acceptable properties for assessing defect clustering

The × symbol represents the index with poor properties for assessing defect clustering

6 Conclusion

The defect distribution, including the number of defects and the clustering pattern on a wafer, significantly influences wafer yield. Besides the number of defects, defect clustering also must be monitored in IC fabrication process control to enhance wafer yield. Defect clustering tends to increase with wafer size. This study developed a CI_M based on the rotating axis technique to assess the degree of defect clustering. The CI_M and other extensively used clustering indices were compared using a simulation experiment to confirm the superiority of the CI_M.

To summarize, this study possesses the following merits:

1. The CI_M has the same advantage as the CI_J in not requiring any statistical assumptions regarding the defects. The CI_M is also sensitive to the percentage of defects in the clustering area.
2. The CI_M values assess the degree of defect clustering accurately, allowing engineers to accurately monitor defects in the IC fabrication process.
3. The CI_M calculation is easy and simple to use for engineers with minimal statistical knowledge.
4. The developed CI_M can be generalized to any wafer size.

References

1. Cunningham JA (1990) The use and evaluation of yield models in integrated circuit manufacturing. IEEE T Semiconduct M 3 (2):60–71
2. Friedman DJ, Hansen MH, Nair VN, James DA (1997) Model-free estimation of defect clustering in integrated circuit fabrication. IEEE T Semiconduct M 10(3):344–359
3. Jun CH, Hong Y, Kim SY, Park KS, Park H (1999) A simulation-based semiconductor chip yield model incorporating a new defect cluster index. Microelectron Reliab 39:451–456
4. Rogers A (1974) Statistical analysis of spatial dispersion: the quadrat method. Pion, London
5. Raghavachari M, Srinivasan A, Sullo P (1997) Poisson mixture yield models for integrated circuits: a critical review. Microelectron Reliab 37(4):565–580
6. Stapper CH (1973) Defect density distribution for LSI yield calculations. IEEE Trans Electron Dev ED-20:655–657
7. Sharma S (1996) Applied multivariate techniques. Wiley, New York